ACS OMEGA

http://pubs.acs.org/journal/acsodf

Article

Green Synthesis of a CuO–ZnO Nanocomposite for Efficient Photodegradation of Methylene Blue and Reduction of 4-Nitrophenol

Aklilu Guale Bekru, Lemma Teshome Tufa, Osman Ahmed Zelekew,* Mahendra Goddati, Jaebeom Lee, and Fedlu Kedir Sabir*

Cite This: *ACS Omega* 2022, 7, 30908–30919

Read Online

ACCESS | Metrics & More | Article Recommendations | Supporting Information

ABSTRACT: CuO–ZnO nanocomposites (NCs) were synthesized using an aqueous extract of *Verbascum sinaiticum* Benth. (GH) plant. X-ray diffraction (XRD), spectroscopic, and microscopic methods were used to explore the crystallinity, optical properties, morphology, and other features of the CuO–ZnO samples. Furthermore, catalytic performances were investigated for methylene blue (MB) degradation and 4-nitrophenol (4-NP) reduction. According to the results, CuO–ZnO NCs with 20 wt % CuO showed enhanced photocatalytic activity against MB dye with a 0.017 min^{-1} rate constant compared to 0.0027 min^{-1} for ZnO nanoparticles (NPs). Similarly, a ratio constant of 5.925 min^{-1} g^{-1} 4-NP reductions was achieved with CuO–ZnO NCs. The results signified enhanced performance of CuO–ZnO NCs relative to ZnO NPs. The enhancement could be due to the synergy between ZnO and CuO, resulting in improved absorption of visible light and reduced electron–hole (e^-/h^+) recombination rate. In addition, variations in the CuO content affected the performance of the CuO–ZnO NCs. Thus, the CuO–ZnO NCs prepared using *V. sinaiticum* Benth. extract could make the material a desirable catalyst for the elimination of organic pollutants.

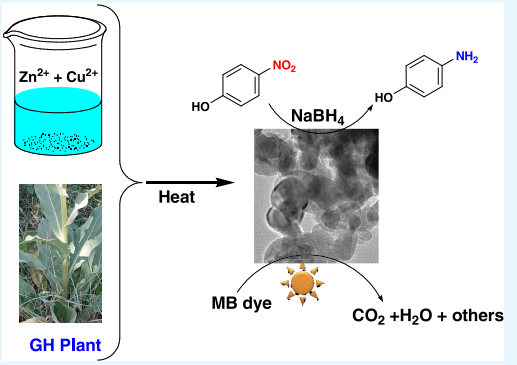

1. INTRODUCTION

Freshwater is one of the most vital resources needed for the well-being of mankind. Nowadays, water pollution has become one of the challenges our world faces, particularly due to toxic and carcinogenic[1,2] soluble organic pollutants released from industries such as textiles,[2,3] paper and pulp,[1,4] pharmaceuticals, and tanneries.[5] Thus, removing these pollutants before releasing effluents into the environment is essential. Conventional wastewater treatment techniques have limitations due to low efficiency, high cost, or generation of secondary contaminants. Therefore, developing eco-friendly, efficient, and low-cost materials and fabrication techniques are necessary.[6] Currently, researchers are exploring the use of nanostructured material-based catalysts as alternatives to conventional techniques. The unique characteristics of nanoscale materials have led to their use as catalysts for the degradation of pollutants into benign compounds.[7,8] Recently, nanostructured material-based photocatalysis has shown remarkable development in the applications of water splitting,[9,10] dye degradation,[11,12] and drug degradation.[13−16] Specifically, metal oxide-based nanostructure photocatalysis is a promising approach for efficiently removing organic contaminants from wastewater.

As a result of their unique properties and versatility, metal oxides (ZnO, TiO_2, WO_3, CuO, Cu_2O, Fe_2O_3, etc.) play a key role in catalysis.[17,18] ZnO is among the metal oxides that have been explored most for wastewater treatment for its low cost, abundant availability, nontoxicity, and favorable exciton binding energy.[19,20] However, wide bandgap for visible light activation, fast e^-/h^+ recombination, and photocorrosion in aqueous media are drawbacks limiting the practical application of pristine ZnO as photocatalyst.[7,19] Several properties have been demonstrated by coupling of ZnO with low-bandgap p-type CuO semiconductors: (i) a p–n heterojunction is formed, which reduces the e^-/h^+ recombination rate;[21] (ii) narrow bandgaps are created, which improve visible light harvesting;[22,23] and (iii) improved reusability without significant performance loss.[24] Therefore, developing CuO–ZnO nanostructured material is necessary to achieve this goal.

CuO–ZnO NCs can be fabricated by various methods including precipitation,[25] sol–gel,[26] solvothermal,[27] electrospinning,[28] photodeposition,[29] microwave-assisted,[30] electro-

Received: April 30, 2022
Accepted: August 18, 2022
Published: August 26, 2022

ACS Publications

© 2022 The Authors. Published by American Chemical Society

Scheme 1. Schematic Diagram of MW-Assisted CuO−ZnO NC Synthesis Using GH

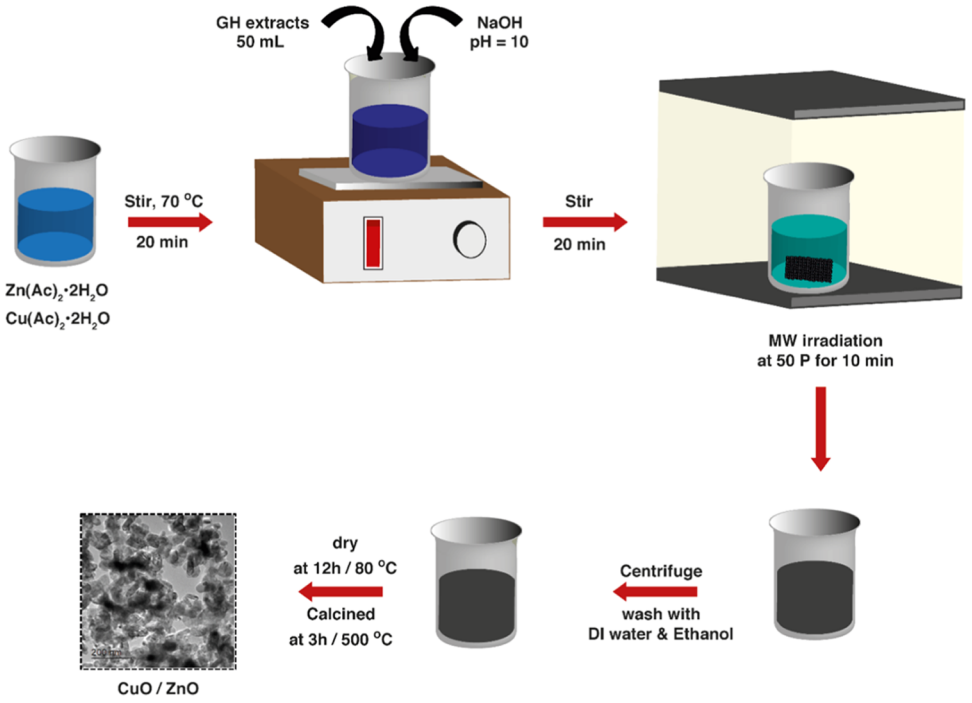

chemical,[31] thermal decomposition,[32] and spray pyrolysis.[33] Among these methods, a microwave-assisted method has several benefits in comparison to conventional heating methods, such as fast reactions, uniform particle size distribution, high yield, and highly pure nanomaterials.[34] For CuO−ZnO NC synthesis, the majority of the methods utilize a variety of precursors as well as other reagents. A green chemistry approach, however, encourages the use of cheap, environmentally benign chemical substances and waste-free methods that eliminate chemical waste.[35] Plant extracts provide biomolecules that are safe, green, cheap, and naturally available.[36,37] Thus, biomolecules are the potential alternative to harsh chemicals.[38] The biomolecules found in the extracts play a crucial role as reducing agents, stabilizing agents, or both, which in turn affect the properties and morphologies of the resulting nanomaterials.[39,40] The nature of the biomolecules greatly affects their interaction with the metal ions.[41] According to the previous reports,[42,43] biomolecule-based metal-oxide NP synthesis involves formation of a biomolecule−metal ion complex, then a metal hydroxide complex, and eventually metal-oxide nanoparticles.

CuO−ZnO NCs synthesis was reported using extracts of plants like *Clerodendrum infortunatum*,[44] *Melissa officinalis* L.,[45] *Vaccinium arctostaphylos* L.,[46] and *Ginkgo biloba*.[47] This study involves preparing CuO−ZnO NCs using GH extract. To our knowledge, there has not yet been a publication on CuO−ZnO NC catalyst synthesized using GH. GH is a medicinal plant and is abundantly available for use in nanoparticle synthesis. As reported, aqueous extracts of GH leaves contain phytochemicals that have significant reducing properties, such as polyphenols and saponins, making GH a promising candidate for nanoparticle synthesis.[48,49] Besides, the polyphenols and saponins with other biomolecules present in the extract can stabilize the nanoparticle formation and control the morphology of the resulting nanostructure. Thus, the use of GH extracts for CuO−ZnO NCs synthesis has valuable importance.

The current work describes a green approach for CuO−ZnO NC synthesis utilizing an aqueous extract of GH with an efficient, low-cost, simple, and rapid MW-assisted method. Microscopy, spectroscopy, and other methods were used to study the resulting samples. The catalytic activity of CuO−ZnO NCs was also evaluated against MB degradation and 4-NP reduction. For comparison purposes, the degradation performance of ZnO was also evaluated. CuO−ZnO NCs prepared with the aid of GH extract are anticipated to have enhanced catalytic reactions due to improved response to visible light and reduced e^-/h^+ recombination rates.

2. EXPERIMENTAL SECTION

2.1. Chemicals and Reagents. Analytic-grade reagents of copper acetate ($Cu(CH_3COO)_2.H_2O$) (99%, UNI-CHEM), zinc acetate ($Zn(CH_3COO)_2.2H_2O$) (99%, UNI-CHEM), sodium borohydride ($NaBH_4$) (95%, SRL), sodium hydroxide ($NaOH$) (98%, Loba), and methylene blue ($C_{16}H_{18}ClN_3S.3H_2O$) (PJ) were used. Leaves of *Verbascum sinaiticum* Benth. were obtained from the Adama Science and Technology University campus, Ethiopia. For the preparation of solution and washing activities, deionized water (DW) was utilized throughout the experiment.

2.2. Extract Preparation. The leaves of the *V. sinaiticum* Benth. plant (Figure S1) were collected, washed in distilled water, air-dried, and then ground to powder using a grinder. Then, 10 g of GH powder and 100 mL of DW were mixed in a 1 L beaker and then left to boil under magnetic stirring for 10 min. After cooling, filtration was used to separate the extract, which was then stored at 4 °C for use in the subsequent experiments.

2.3. Synthesis of the CuO−ZnO NCs. CuO−ZnO NCs were synthesized by the MW-assisted method using $Zn(CH_3COO)_2.2H_2O$, $Cu(CH_3COO)_2{\cdot}H_2O$, and GH leaf

https://doi.org/10.1021/acsomega.2c02687
ACS Omega 2022, 7, 30908−30919

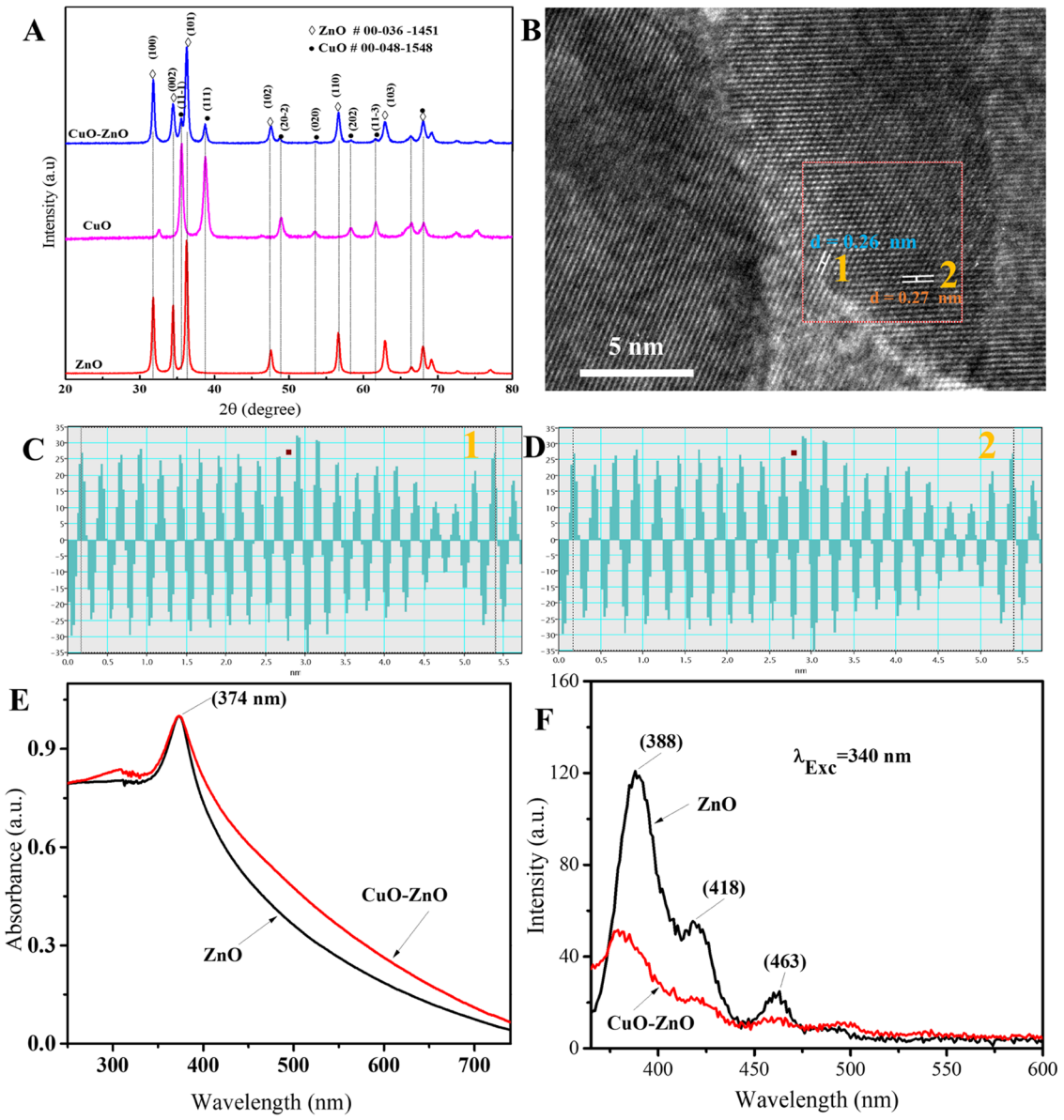

Figure 1. (A) XRD pattern of ZnO, CuO, and CuO−ZnO, (B) lattice fringe of CuO−ZnO NCs, (C, D) *d*-spacing average of ZnO (1), and CuO (2) in CuO−ZnO NCs, (E) absorption spectra of ZnO and CuO−ZnO, and (F) PL spectra of ZnO and CuO−ZnO samples.

extract, following the reported procedure.[46] Typically, 5.0 g of $Zn(CH_3COO)_2{\cdot}2H_2O$ and 1.25 g of $Cu(CH_3COO)_2.H_2O$ were dissolved in DW and heated at 75 °C under stirring. While it is being stirred, 50 mL of extract was slowly added to the solution. NaOH (20 wt %) was used for adjusting the pH and then stirred for 20 min. Subsequently, the mixture was MW-irradiated using a household oven (1000 W, Comet) for 10 min at 50% power output. After purification with ample DW and ethanol, the brown precipitate obtained was dried at 80 °C for 12 h. A pestle was used to hand-crush the resultant solid. Eventually, calcination of the powder was conducted at 500 °C for 3 h using a muffle furnace. The resulting product was a 20 wt % CuO content sample.

Similarly, other samples with CuO contents of 0% (ZnO), 10% (CuO−ZnO), 30% (CuO−ZnO), 50% (CuO−ZnO), and 100% (CuO) by wt % were prepared using zinc acetate (6.25, 5.65, 4.25, 3.05, and 0 g) and copper acetate (0, 0.65, 1.9, 3, and 5.75 g), respectively. To each of these mixtures, 50 mL of extract was added. The concentration of $[Cu^{2+} + Zn^{2+}]$ and the total volume of the final solution were kept constant. The remaining procedures were similar to that of the 20 wt % CuO. Scheme 1 provides the schematic summary of the CuO−ZnO NC synthesis.

2.4. Characterizations. The crystallinity and crystal phase of the obtained powder was probed by an X-ray diffraction (XRD) instrument (XRD-7000S Shimadzu) with Cu Kα radiation. The elemental composition on the surface was collected using an X-ray photoelectron spectroscope (XPS, Thermo Scientific, Al Kα ($h\nu$ = 1350 eV)). The surface morphology and elemental mapping were measured by a field emission scanning electron microscope (FESEM; HITACHI, S-4800) and a transmission electron microscope (TEM; FEI Tecnai G2 F30). UV−visible spectral characterization of the nanomaterials was performed using a UV−vis spectrophotometer (JASCO V-670). The emission spectra were measured using a fluorescence spectrophotometer (Agilent Cary Eclipse Fluorescence Spectrophotometer). The surface area analysis was conducted using a Micromeritics ASAP 2420 (V2.09 J)

https://doi.org/10.1021/acsomega.2c02687
ACS Omega 2022, 7, 30908−30919

instrument by N_2 adsorption at 77 K. The progress of degradation and reduction reactions was observed by a UV−vis spectrophotometer (Azzota: SM-1600).

2.5. Photocatalytic Performance Test. The photocatalytic efficiency of the CuO−ZnO NC sample was evaluated against the MB degradation (with a 150 W halogen lamp). The reaction suspension was prepared by mixing 120 mL of MB (10 ppm) and 20 mg of catalyst. To assure homogeneous dispersion of the catalyst and dye molecules, a 30-min sonication was used. Then, it was irradiated by visible light while being magnetically stirred continuously. Every 15 min, a 4 mL of sample was taken and centrifuged to separate the catalysts from the liquid before the absorbance measurement. After photocatalytic degradation of MB, the absorbance of each sample was measured. The percentage of photocatalytic degradation (D%) and rate of reaction were evaluated using eqs 1 and 2, respectively.[11,50]

$$D(\%) = \frac{C_0 - C_t}{C_0} \times 100 \quad (1)$$

$$\ln\left(\frac{C_t}{C_0}\right) = -kt \quad (2)$$

where k represents rate constant, and C_0 and C_t are the dye (pollutant) concentrations before (or at time = 0 min) and after illumination (or at time = t min), respectively.

2.6. Catalytic Reduction Test. To assess the catalytic capability of CuO−ZnO, 4-NP was used as a test nitroaromatic compound in the presence of $NaBH_4$ as a reductant. Typically, 40 mg of $NaBH_4$ and 40 mg of catalyst were dispersed in a 250 mL beaker containing 100 mL of 20 ppm 4-NP. The reduction progress was tracked by a UV−vis spectrophotometer.[51] Every 3 min, 3 mL sample of the mixture was withdrawn and its absorbance spectrum was then collected. Furthermore, the rate of reduction was evaluated using eq 2.

3. RESULTS AND DISCUSSION

The crystallinity and crystal phase of the calcined samples were investigated using the data from XRD measurements. XRD patterns of CuO, ZnO, and CuO−ZnO samples are shown in Figure 1A. As displayed in the figure, the XRD patterns of the ZnO sample at the 2θ values of 31.79, 34.45, 36.26, 47.58, 56.6, 62.88, 66.4, 67.98, and 69.11 were indexed as (100), (002), (101), (102), (110), (103), (200), (112), and (201), respectively, corresponding to the hexagonal ZnO phase (card no. 00-036-1451). Similarly, the diffraction peaks of CuO sample obtained at the 2θ values of 32.48, 35.62, 38.78, 48.94, 53.5, 58.29, 61.7, 65.9, 66.4, 68.08, and 72.46 indexed as (110), (11−1), (111), (20−2), (020), (202), (11−3), (022), (31−1), (220), and (311) planes, respectively, were assigned to the monoclinic CuO phase (card no. 00-048-1548). Moreover, the diffraction peaks of CuO−ZnO NCs observed at the 2θ values of 31.76, 34.4, 36.28, 47.58, 56.62, 62.84, 66.36, 67.98, and 69.14 matched with the ZnO phase and those at the 2θ values of 35.54, 38.72, 48.74, 53.42, 58.33, 61.6 matched with the CuO phase, confirming the formation of CuO−ZnO. The diffraction patterns of the composite do not contain peaks other than CuO and ZnO, indicating that the prepared sample is free of impurities.[52] Following examination by high-resolution TEM, the lattice fringes for ZnO−CuO were observed. Figure 1C,D displays the line intensity profile for the selected lines in the inverse fast Fourier transform (IFFT) image of the CuO−ZnO NC sample corresponding to the d-spacing average of 0.26 nm (Figure 1C) and 0.27 nm (Figure 1D). According to the results, 0.26 nm is the interplanar spacing between the (002) plane of hexagonal ZnO (card no. 000-036-1451), while 0.27 nm is the spacing between the (110) plane of monoclinic CuO (card no. 00-048-1548) (Figure 1 B−D). This result is very consistent with the literature reports[29,53] and XRD analysis.

The average crystallite size was determined using Scherrer's formula (eq 3) for the first three intense peaks: (100), (002), and (101) for ZnO; (11−1), (111), and (20−2) for CuO; and (100), (002), and (101) for the CuO−ZnO NCs.[54] The calculated average crystallite sizes were 22, 14, and 18 nm for ZnO, CuO, and CuO−ZnO samples, respectively. The values obtained indicated that the synthesized samples have crystallites in the nanosize range. In view of the possibility that photocatalysts could be improved by reducing the crystallites size, the nanosize range crystallites of the synthesized CuO−ZnO samples make the materials an attractive photocatalyst candidate.[55]

$$D = \frac{0.9\lambda}{\beta \cos(\theta)} \quad (3)$$

where λ stands for the wavelength of the incident X-ray, θ stands for the diffraction angle, and β represents the peak width at half-maximum of its height corresponding to the peak on the XRD pattern.

The absorption spectra of ZnO and CuO−ZnO in the UV−vis range are given in Figure 1E. Both ZnO and CuO−ZnO NC samples absorb strongly in the UV region (λ_{max} = 374 nm), which is consistent with previous works.[56,57] Portions of the absorption spectrum fall in the visible range with the tail reaching 800 nm, which could be attributed to the light scattering in the colloidal suspension.[56] In comparison to pristine ZnO NPs, the CuO−ZnO sample showed a broader absorption spectrum over the range of 250−800 nm. The presence of CuO is responsible for a broader absorbance in the visible region,[58] indicating enhanced absorption capacity of the CuO−ZnO NCs in the visible light range. The bandgap calculated from Tauc's formula[12,33] was approximately 3.01 eV for ZnO and 2.74 eV for the CuO−ZnO NCs (Figure S2). The result showed that the bandgap of the CuO−ZnO NCs is lower than ZnO NPs alone. The improved efficiency of visible light-harvesting capacity makes CuO−ZnO NCs suitable candidates for photocatalytic applications.[59]

The photoluminescence (PL) properties of ZnO and CuO−ZnO suspension in methanol are displayed in Figure 1F. When the samples are excited at 340 nm, the PL spectra showed a strong emission band around 388 nm and relatively weaker emission band around 463 nm, including a shoulder band around 418 nm. The strong narrow emission band around 388 nm was attributed to the exciton recombination corresponding to the near band edge,[60] whereas the other peaks that appeared around 418 and 463 nm could be originated from the deep-level defects.[61] Since PL emission is induced when the photogenerated e^-/h^+ recombine, the relatively lower PL intensity of the CuO−ZnO NCs compared to ZnO NPs indicated the decreased radiative recombination rate in the composite, which could be attributed to the better e^-/h^+ separation and prolonged exciton lifetime.[60] Thus, coupling CuO and ZnO revealed a decreased rate of exciton recombination with improved visible light absorption.[62]

https://doi.org/10.1021/acsomega.2c02687
ACS Omega 2022, 7, 30908−30919

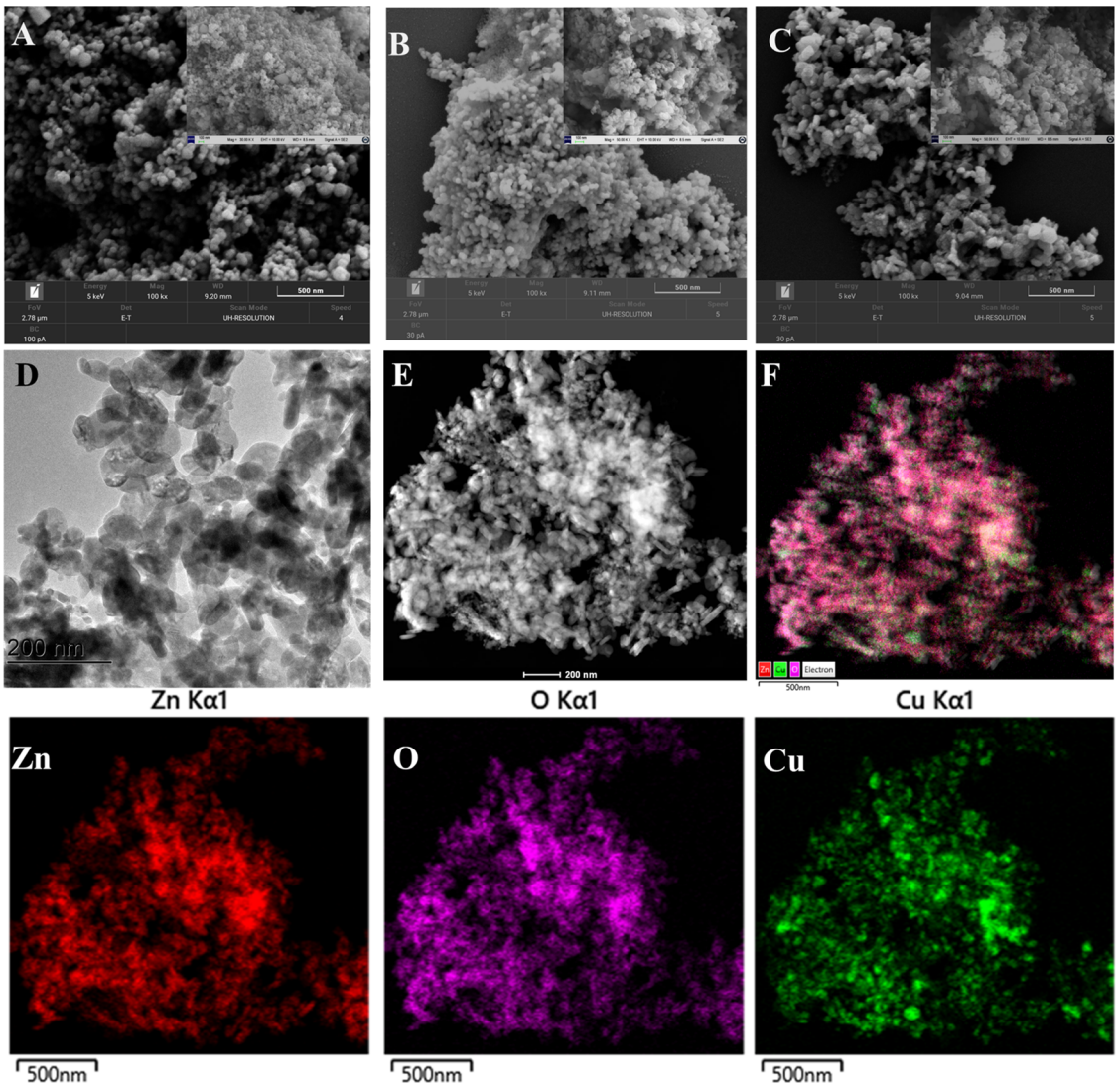

Figure 2. SEM images: ZnO (A), CuO (B), and CuO−ZnO (C); (D) TEM image of CuO−ZnO, (E) HAADF-STEM, (F) EDS layered mappings, and EDS elemental mappings: zinc (Zn), copper (Cu), and oxygen (O).

Figure 2A−C illustrates SEM images of the synthesized catalysts using GH extract. The micrograms indicated that ZnO and CuO were found in a cluster of spherical-like NPs, while CuO−ZnO NCs were found in a plate-like morphology. The morphology and crystal structure of the CuO−ZnO sample was further evaluated by TEM analysis, as displayed in Figures 2D and S3. The results illustrated that the prepared CuO−ZnO NCs possess plate-like nanostructures, supporting the SEM analysis. Furthermore, the distribution of CuO and ZnO in CuO−ZnO NCs was evaluated from EDS mapping images. The typical high-angle annular dark-field scanning transmission electron microscopy (HAADF-STEM) image and corresponding EDS mapping of CuO−ZnO NCs (Figure 2E,F) and Figure S4 demonstrated the even distribution of O, Cu, and Zn elements throughout the CuO−ZnO sample.[63]

XPS study was utilized for the survey of oxidation states and compositions of the CuO−ZnO sample surface. The resulting XPS spectrum of the CuO−ZnO sample is presented in Figure 3. The peaks observed in the full survey spectrum displayed in Figure 3A indicate the presence of O, Cu, and Zn species. As shown in Figure 3B, XPS peaks at 1021.68 and 1044.77 eV were assigned to the Zn energy levels designated as $2p_{3/2}$ and $2p_{1/2}$, respectively.[64] Similarly, the peaks centered at 933.1 and 953.01 eV were related to the $2p_{3/2}$ and $2p_{1/2}$ levels of Cu, respectively (Figure 3C).[62] Satellite peaks appeared at the upper energy sides, 942.96 and 940.68 eV for Cu $2p_{3/2}$ and 961.56 eV for Cu $2p_{1/2}$ (Figure 3C), confirming the existence of Cu in Cu^{2+} state, i.e., CuO.[65] Furthermore, the peak located at 530.18 eV is attributed to the O 1s from the lattice oxygen (O^{2-}) bound to metals, and the shoulder peak at 531.67 corresponds to the oxygen (O^{2-}) in the oxygen-deficient region indicating the presence of oxygen vacancy (O_V). Hence, the XPS study revealed the presence of CuO and ZnO in the CuO−ZnO sample, which is consistent with the results from XRD, HRTEM, and EDS elemental mapping studies.

The adsorption−desorption isotherm of N_2 for the CuO−ZnO NC sample exhibited type IV isotherm having narrow adsorption−desorption of H3-type hysteresis loops (Figure S6), indicating the presence of a mesoporous structure.[66−68] The BET analysis indicated an approximate specific surface area of 18.49 $m^2\ g^{-1}$ in the P/P_0 range of 0.05−0.3. Similarly, a 23.78 nm adsorption average pore size was obtained from the BET method. The corresponding distribution of the pore sizes from the Barrett−Joyner−Halenda (BJH) method (inset of

https://doi.org/10.1021/acsomega.2c02687
ACS Omega 2022, 7, 30908−30919

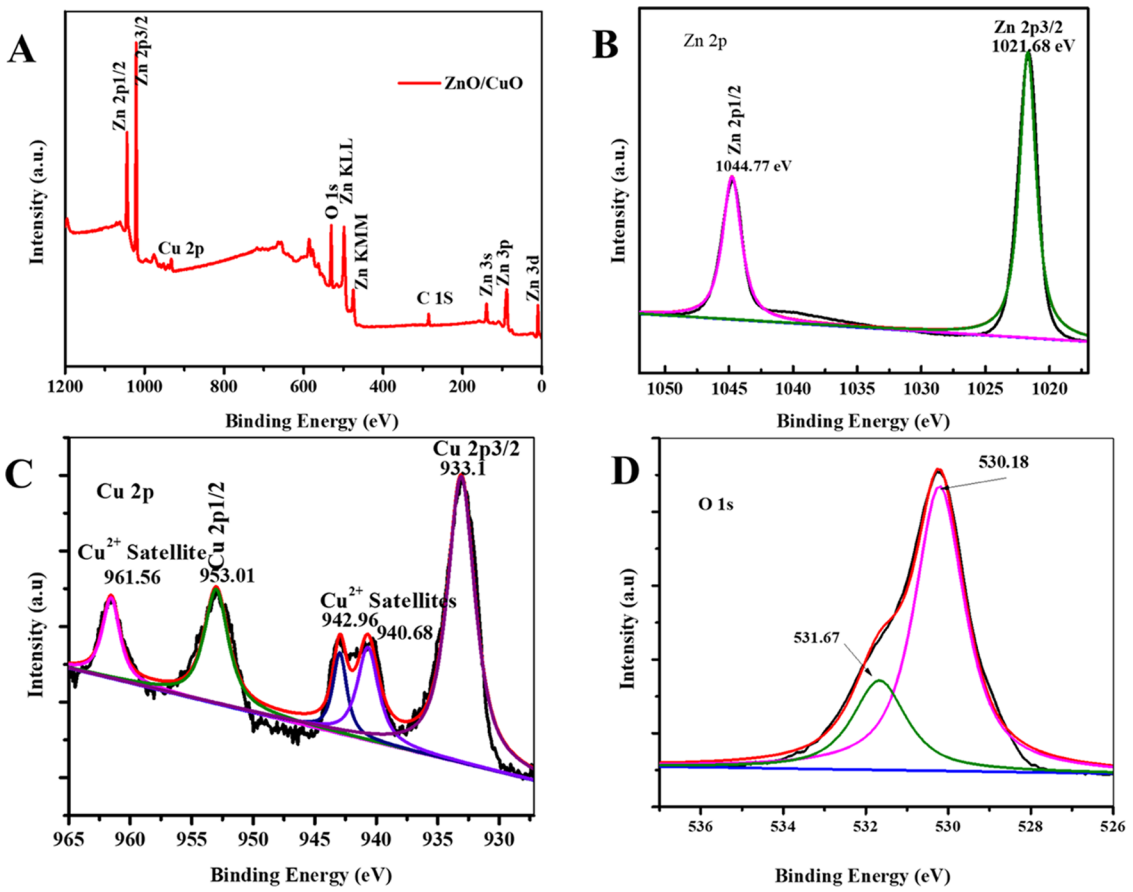

Figure 3. XPS spectra of CuO−ZnO NCs: (A) full survey, (B) Zn 2p, (C) Cu 2p, and (D) O 1s.

Figure S6) indicated that the textural porosity of CuO−ZnO NCs falls under the mesoporous materials.

The photocatalytic activities of CuO−ZnO NCs were tested against MB degradation using visible light, and the corresponding results are given in Figure 4. The UV−vis absorbance of MB showed a strong peak at 664 nm.[47] In the presence of catalysts, irradiating MB aqueous solution with visible light resulted in decreasing absorbance with time, indicating photodegradation of the MB. More specifically, the CuO−ZnO NCs showed improved photocatalytic performance compared to the pristine ZnO NPs with an efficiency of 24% for ZnO and 82% for CuO−ZnO NCs, as shown in Figure 4A−D. The rate constant (k) calculated from the linear fitted plots of $\ln(C_t/C_0)$ *vs* time (Figure 4D) was found to be 0.0027 and 0.017 min^{-1} for ZnO and CuO−ZnO NCs, respectively. The enhanced performance could be the result of coupling a p-type CuO with an n-type ZnO. Specifically, the improved visible light absorption capacity of CuO−ZnO (from UV−vis analysis), and the minimized rate of e^-/h^+ recombination (from PL analysis) are responsible for the enhancement.[19]

A study on how the CuO contents affect the activity of the prepared catalyst against MB was also conducted by varying CuO contents. The results depicted in Figure 5A−C show the performance of 24, 65, 82, 75, and 76% MB degradation for CuO wt % of 0, 10, 20, 30, and 50% samples of CuO−ZnO NCs, respectively. The calculated rate constants were 0.0027, 0.0112, 0.0170, 0.0139, and 0.0144 min^{-1} for ZnO (0%), CuO−ZnO (10%), CuO−ZnO (20%), CuO−ZnO (30%), and CuO−ZnO (50%) contents of CuO, respectively (Figure 5D). While all CuO−ZnO samples showed higher performance than the ZnO NPs alone, CuO−ZnO NCs with 20 wt % CuO displayed the highest performance. This implies that there exists an optimum amount of CuO component in CuO−ZnO beyond which photocatalytic activity diminishes.[69] As reported in previous studies, the decreased performance of CuO−ZnO with increased CuO content beyond the optimum value could be explained by the increased agglomeration of CuO that masks surface photoactive sites or enhances the rate of e^-/h^+ recombination.[70]

In general, the processes involved in photocatalysis include absorption of light, e^-/h^+ pairs generation and separation, transfer of e^-/h^+ to the active sites for a redox reaction, recombination of e^-/h^+, and adsorption/desorption of reactants/products. Depending on the redox reaction between the charge carriers and the adsorbed species or surrounding species, reactive oxygen species (ROS) like hydroxyl radicals ($^{\bullet}OH$), superoxide anion radicals ($O_2^{\bullet-}$), singlet oxygen species ($^1O_2$), and peroxide molecules (H_2O_2) may form.[7,8] These species have a high tendency of oxidizing organic pollutants into less-toxic substances or mineralize them into CO_2, H_2O, and others.

In the case of CuO−ZnO NCs, light of appropriate energy illumination generates exciton, where e^- accumulate in the conduction band (CB) and h^+ in the valance band (VB). Coupling CuO with ZnO semiconductor provides the band alignment in which the e^- in the CB of CuO are pushed to the relatively less negative CB of ZnO. Thus, the h^+ in the VB oxidizes H_2O/HO^- (or organic pollutant RH) resulting in $HO^{\bullet}$ (or $R^{\bullet}$) depending on the potential of the hole in the VB

https://doi.org/10.1021/acsomega.2c02687
ACS Omega 2022, 7, 30908−30919

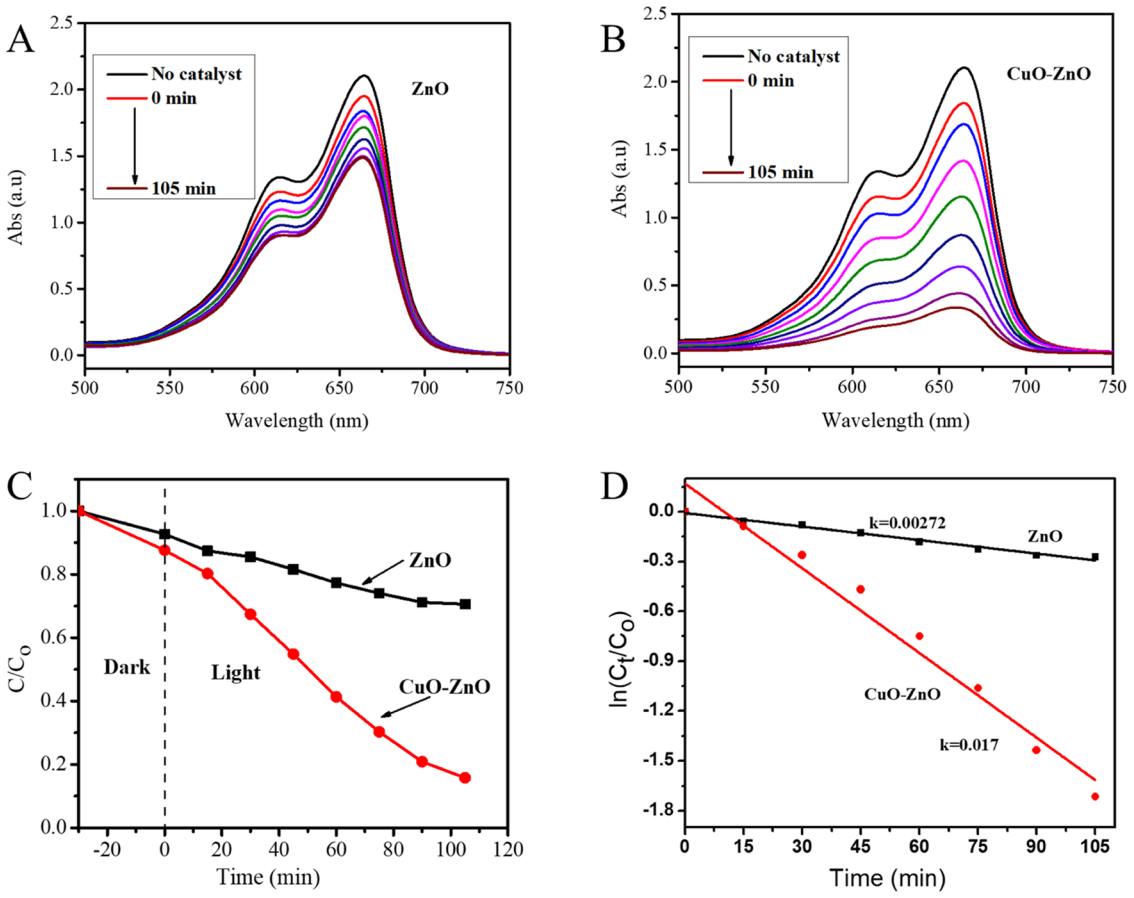

Figure 4. (A, B) Photocatalytic removal of MB using ZnO (A) and CuO−ZnO (B), (C) plots of C_t/C_0 *vs* reaction time (min), and (D) plots of $\ln(C_t/C_0)$ *vs* reaction time (min) for MB degradation using ZnO and CuO−ZnO.

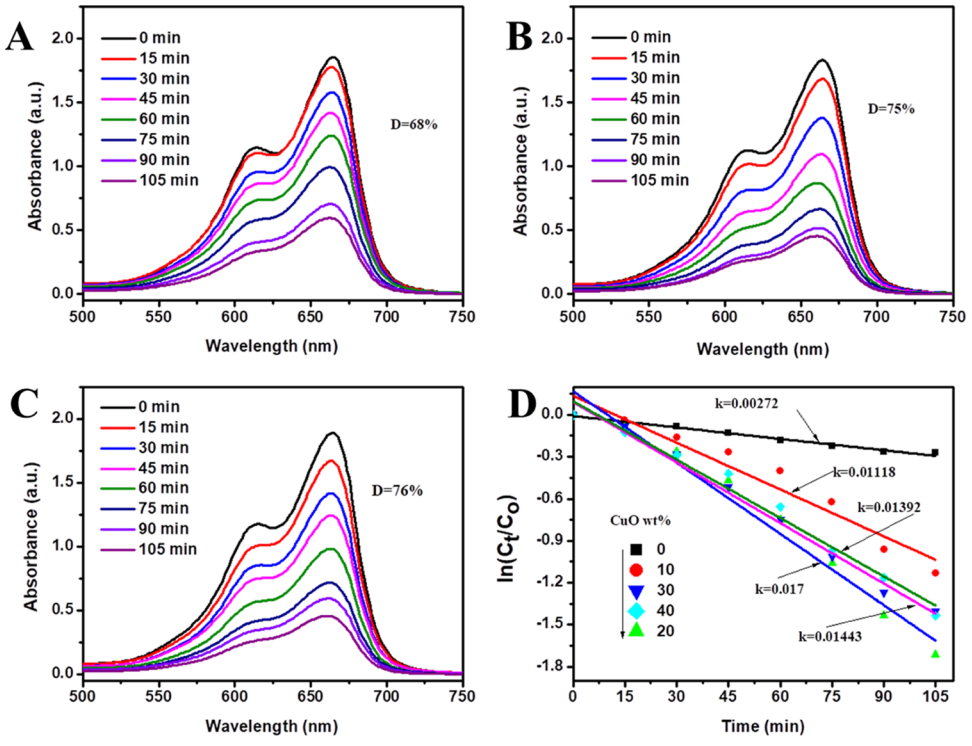

Figure 5. Photocatalytic degradation of MB using CuO−ZnO with different CuO wt % (A) 10%, (B) 30%, (C) 50%, and (D) the effect of CuO wt % content on the apparent rate constant CuO−ZnO for MB degradation.

https://doi.org/10.1021/acsomega.2c02687
ACS Omega 2022, 7, 30908−30919

Table 1. Comparison of the CuO−ZnO Photocatalyst Synthesized Using GH with Previously Reported ZnO-Based NCs for Photocatalytic Degradation of MB

	experimental conditions			performance		
catalyst	amount of catalyst (mg)	concentration of MB	light	rate const., k (min^{-1})	ratio const., K (min^{-1} g^{-1})	ref
CuO−ZnO	25	10^{-3} M	vis	0.0235	0. 94	20
Cr_2O_3/ZnO	25	10 ppm (125 mL)	vis	0.015	0.6	72
ZnO/CuO	40	20 ppm	vis	0.022.3	0.56	73
CuO−ZnO	50	15 ppm (100 mL)	UV	0.01948	0.39	74
CuO−ZnO	20	20 ppm	vis	0.017	0.85	this work

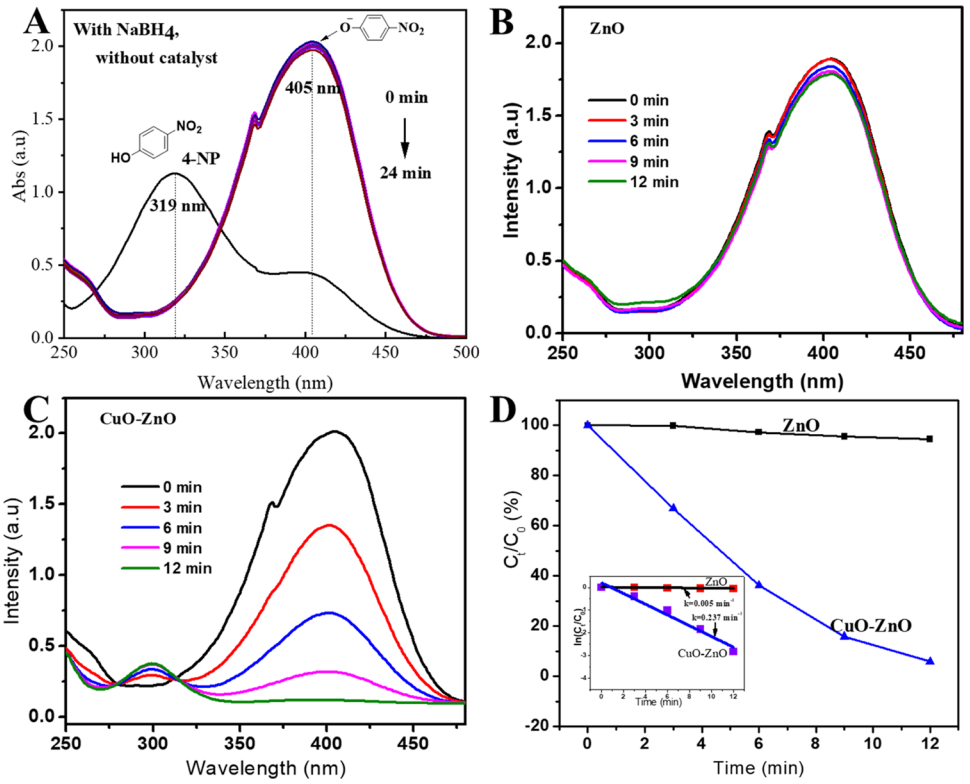

Figure 6. (A) Absorption spectrum of 4-NP with and without $NaBH_4$, (B, C) reduction of 4-NP with $NaBH_4$ in the presence of catalysts: ZnO(B) and CuO−ZnO(C), and (D) plots of C_t/C_0 *vs* reaction time (min) (inset: plot of $\ln(C_t/C_0)$ *vs* t (min)) for 4-NP reduction kinetics.

(eq 4). Similarly, the e^- in the CB will be trapped by the dissolved oxygen and produce ROS that finally degrades the pollutant (eq 4).[47] Hence, the complete degradation of MB ends up producing H_2O, CO_2, and other inorganic ions like NO_3^-, SO_4^{2-}, and Cl^-, as shown in eq 5.[71]

$$\text{CuC} - \text{ZnO} + h\nu \rightarrow h^+/e^- \xrightarrow{H_2O/OH^-/O_2} \text{ROS} \quad (4)$$

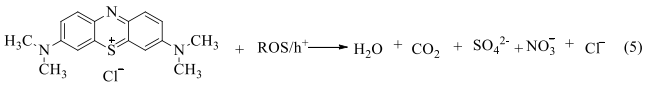

(5)

Table 1 compares the activities of this work to the earlier reports using ZnO-based NCs against MB degradation under different experimental conditions. Despite the different experimental conditions, the CuO−ZnO NCs obtained using GH exhibited superior photocatalytic performance compared to the previously reported literature values based on their ratio constants (Table 1). It degraded 82% of the initial MB amount within 105 min with a rate constant of 0.017 min^{-1} or ratio constant of 0.85 min^{-1} g^{-1} (ratio of k to the mass of catalyst).

Furthermore, the catalytic reduction activity of the nanostructured catalysts was also tested for 4-NP along with the strong reducing agent $NaBH_4$. Figure 6 shows the progress of reduction and corresponding kinetics in the presence of ZnO and CuO−ZnO catalysts. The aqueous solution of 4-NP displayed an absorbance peak at 320 nm (Figure 6A). Upon $NaBH_4$ addition, the peak at 320 nm (from light yellow solution) disappeared, while a strong peak around 405 nm (intense yellowish-orange solution) was observed, indicating the formation of 4-nitrophenolate ion in alkaline media (Figure 6A). The peak at 405 nm showed no change in intensity over an hour. However, when ZnO and CuO−ZnO were added, the peak intensity at 405 nm drops, while a new peak at 300 nm emerges, confirming the 4-AP formation. CuO−ZnO NCs showed strong catalytic efficiency with reaction completion in less than 12 min (Figure 6B,C). On the other hand, ZnO showed insignificant change in the 4-nitrophenolate ion (in 12 min), suggesting the lower catalytic performance of ZnO than CuO−ZnO NCs against the reduction of 4-NP.

The reduction kinetics of 4-NP with $NaBH_4$ and catalysts is shown in Figure 6D. The rate constants of the reduction reaction were obtained from the linear fitted plot of $\ln(C_t/C_0)$ *vs* time of reaction, as depicted in Figure 6D (inset) applying eq 2. In this regard, the ratio constants (K) of 0.125 and 5.925

https://doi.org/10.1021/acsomega.2c02687
ACS Omega 2022, 7, 30908−30919

Scheme 2. Presumed Catalytic Reaction Mechanism of 4-NP Reduction Using CuO−ZnO NCs as a Catalyst

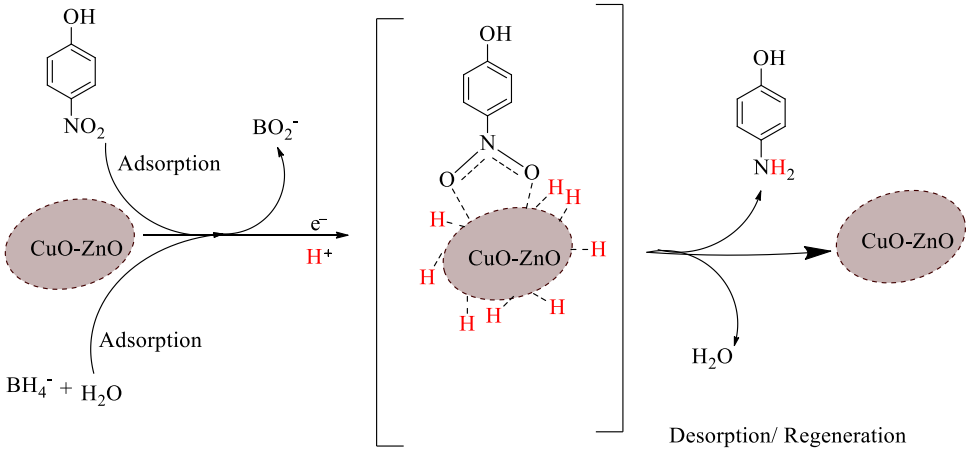

min^{-1} g^{-1} were obtained for ZnO and CuO−ZnO nanocatalysts, respectively.[64]

The reduction of 4-NP into 4-AP by $NaBH_4$ is a thermodynamically feasible reaction.[51] However, the rate of reduction reaction is slow due to the kinetic barrier in the reaction steps.[51] Catalysts allow the reaction to take routes with relatively lower energy barriers leading to a faster rate of reaction. Nanostructured catalysts were often used to accelerate the reduction of 4-NP into 4-AP by $NaBH_4$. The proposed reaction mechanism for the conversion of 4-NP into 4-AP by $NaBH_4$ along with CuO−ZnO NCs catalysts is given in Scheme 2. Generally, the mechanisms involve processes such as adsorption/desorption and transfer of electrons and protons. From the aqueous solution, BH_4^- and 4-NP adsorb on the surface of the catalyst, where electron and proton transfers take place. Electrons transfer from BH_4^- to the adsorbed 4-NP through the CuO−ZnO catalyst leading to reduction.[75] Similarly, the protons transfer from the BH_4^- and aqueous solution to the 4-NP, completing the reduction reaction.[76] The adsorption process and transfer of charged species are facilitated by the built-in electric field of the p−n heterojunction of CuO−ZnO.[51] After completion of the redox reaction, the desorption step takes place, as shown in Scheme 2.

The prepared CuO−ZnO NCs have shown good recyclability up to four cycles against the MB using visible light and 4-NP reduction using $NaBH_4$ (Figure S5).

4. CONCLUSIONS

CuO−ZnO NCs have been prepared successfully using the MW-assisted method with GH extract. The synthesized sample was characterized using various techniques. The analysis indicated that crystalline CuO−ZnO NCs with plate-like morphology were obtained. Similarly, the XRD patterns, EDS elemental mappings, and XPS spectra confirmed that the composite was composed of CuO and ZnO with uniform distribution. And also, the UV−vis absorbance and PL analysis of the CuO−ZnO NCs showed enhanced absorption in the visible range with a suppressed recombination rate of e^-/h^+ compared to the ZnO NPs. Furthermore, the prepared sample showed improved photocatalytic degradation of MB and catalytic reduction of 4-NP with rate constants of 0.017 and 0.237 min^{-1}, respectively. Therefore, CuO−ZnO NCs obtained using abundantly available GH extract could be used for the remediation of water polluted by organic dyes.

■ ASSOCIATED CONTENT

Supporting Information

The Supporting Information is available free of charge at https://pubs.acs.org/doi/10.1021/acsomega.2c02687.

Photographic image of *Verbascum sinaiticum* Benth. plant; Tauc's plot of ZnO and CuO−ZnO; TEM, HRTEM, and fast Fourier transform (FFT) of CuO−ZnO NCs; EDS spectrum of CuO−ZnO; recyclability; and N_2 adsorption−desorption isotherms; and BJH pore size distributions of CuO−ZnO NC samples (PDF)

■ AUTHOR INFORMATION

Corresponding Authors

Osman Ahmed Zelekew − *Department of Materials Science and Engineering, Adama Science and Technology University, Adama 1888, Ethiopia;* orcid.org/0000-0003-2633-5426; Email: osman.ahmed@astu.edu.et, osmax2007@gmail.com

Fedlu Kedir Sabir − *Department of Applied Chemistry, Adama Science and Technology University, Adama 1888, Ethiopia*; Email: fedluked130@gmail.com

Authors

Aklilu Guale Bekru − *Department of Applied Chemistry, Adama Science and Technology University, Adama 1888, Ethiopia*

Lemma Teshome Tufa − *Department of Applied Chemistry, Adama Science and Technology University, Adama 1888, Ethiopia; Research Institute of Materials Chemistry, Chungnam National University, Daejeon 34134, Republic of Korea;* orcid.org/0000-0001-6929-8464

Mahendra Goddati − *Department of Chemistry, Chemistry Engineering and Applied Chemistry, Chungnam National University, Daejeon 34134, Republic of Korea*

Jaebeom Lee − *Department of Chemistry, Chemistry Engineering and Applied Chemistry, Chungnam National University, Daejeon 34134, Republic of Korea;* orcid.org/0000-0002-4563-2883

https://doi.org/10.1021/acsomega.2c02687
ACS Omega 2022, 7, 30908−30919

Complete contact information is available at:
https://pubs.acs.org/10.1021/acsomega.2c02687

Notes

The authors declare no competing financial interest.

■ ACKNOWLEDGMENTS

The authors would like to thank the Postgraduate Program of Adama Science and Technology University, Research and Technology Transfer Office, Adama Science and Technology University (No. ASTU/AS-R/013/2021), and Wachemo University for financially supporting this research. They also acknowledge the National Research Foundation of Korea (NRF-2021H1D3A2A01099457).

■ REFERENCES

(1) Mandeep; Gupta, G. K.; Liu, H.; Shukla, P. Pulp and Paper Industry−Based Pollutants, Their Health Hazards and Environmental Risks. *Curr. Opin. Environ. Sci. Heal.* **2019**, *12*, 48−56.
(2) Sivaram, N. M.; Gopal, P. M.; Barik, D. Toxic Waste from Textile Industries. In *In Energy from Toxic Organic Waste for Heat and Power Generation*; Elsevier, 2018; pp 43−54.
(3) Carmen, Z.; Daniel, S. Textile Organic Dyes − Characteristics, Polluting Effects and Separation/Elimination Procedures from Industrial Effluents − A Critical Overview. In *Organic Pollutants Ten Years After the Stockholm Convention - Environmental and Analytical Update*; InTech, 2012; pp 55−86, DOI: 10.5772/32373.
(4) Ilyas, M.; Ahmad, W.; Khan, H.; Yousaf, S.; Yasir, M.; Khan, A. Environmental and Health Impacts of Industrial Wastewater Effluents in Pakistan: A Review. *Rev. Environ. Health* **2019**, *34*, 171−186.
(5) Kanu, I.; Achi, O.K. Industrial Effluents and Their Impact on Water Quality Of Receiving Rivers In Nigeria. *J. Appl. Technol. Environ. Sanit.* **2011**, *1*, 75−86.
(6) Ibrahim, R. K.; Hayyan, M.; AlSaadi, M. A.; Hayyan, A.; Ibrahim, S. Environmental Application of Nanotechnology: Air, Soil, and Water. *Environ. Sci. Pollut. Res.* **2016**, *23*, 13754−13788.
(7) Ong, C. B.; Ng, L. Y.; Mohammad, A. W. A Review of ZnO Nanoparticles as Solar Photocatalysts: Synthesis, Mechanisms and Applications. *Renewable Sustainable Energy Rev.* **2018**, *81*, 536−551.
(8) Nosaka, Y.; Nosaka, A. Y. Generation and Detection of Reactive Oxygen Species in Photocatalysis. *Chem. Rev.* **2017**, *117*, 11302−11336.
(9) Shi, W.; Li, M.; Huang, X.; Ren, H.; Yan, C.; Guo, F. Facile Synthesis of 2D/2D $Co_3(PO_4)_2$/g-C_3N_4 Heterojunction for Highly Photocatalytic Overall Water Splitting under Visible Light. *Chem. Eng. J.* **2020**, *382*, No. 122960.
(10) Momeni, M. M.; Ghayeb, Y. Visible Light-Driven Photoelectrochemical Water Splitting on ZnO−TiO_2 Heterogeneous Nanotube Photoanodes. *J. Appl. Electrochem.* **2015**, *45*, 557−566.
(11) Momeni, M. M.; Ghayeb, Y.; Menati, M. Facile and Green Synthesis of CuO Nanoneedles with High Photo Catalytic Activity. *J. Mater. Sci. Mater. Electron.* **2016**, *27*, 9454−9460.
(12) Momeni, M. M. Fabrication of Copper Decorated Tungsten Oxide-Titanium Oxide Nanotubes by Photochemical Deposition Technique and Their Photocatalytic Application under Visible Light. *Appl. Surf. Sci.* **2015**, *357*, 160−166.
(13) Guo, F.; Huang, X.; Chen, Z.; Cao, L.; Cheng, X.; Chen, L.; Shi, W. Construction of Cu_3P-$ZnSnO_3$-g-C_3N_4 p-n-n Heterojunction with Multiple Built-in Electric Fields for Effectively Boosting Visible-Light Photocatalytic Degradation of Broad-Spectrum Antibiotics. *Sep. Purif. Technol.* **2021**, *265*, No. 118477.
(14) Shi, W.; Shu, K.; Sun, H.; Ren, H.; Li, M.; Chen, F.; Guo, F. Dual Enhancement of Capturing Photogenerated Electrons by Loading CoP Nanoparticles on N-Deficient Graphitic Carbon Nitride for Efficient Photocatalytic Degradation of Tetracycline under Visible Light. *Sep. Purif. Technol.* **2020**, *246*, No. 116930.
(15) Shi, W.; Yang, S.; Sun, H.; Wang, J.; Lin, X.; Guo, F.; Shi, J. Carbon Dots Anchored High-Crystalline g-C_3N_4 as a Metal-Free Composite Photocatalyst for Boosted Photocatalytic Degradation of Tetracycline under Visible Light. *J. Mater. Sci.* **2021**, *56*, 2226−2240.
(16) Shi, W.; Liu, C.; Li, M.; Lin, X.; Guo, F.; Shi, J. Fabrication of Ternary Ag_3PO_4/$Co_3(PO_4)_2$/g-C_3N_4 Heterostructure with Following Type II and Z-Scheme Dual Pathways for Enhanced Visible-Light Photocatalytic Activity. *J. Hazard. Mater.* **2020**, *389*, No. 121907.
(17) Velempini, T.; Prabakaran, E.; Pillay, K. Recent Developments in the Use of Metal Oxides for Photocatalytic Degradation of Pharmaceutical Pollutants in Water—a Review. *Mater. Today Chem.* **2021**, *19*, No. 100380.
(18) Danish, M. S. S.; Estrella, L. L.; Alemaida, I. M. A.; Lisin, A.; Moiseev, N.; Ahmadi, M.; Nazari, M.; Wali, M.; Zaheb, H.; Senjyu, T. Photocatalytic Applications of Metal Oxides for Sustainable Environmental Remediation. *Metals* **2021**, *11*, No. 80.
(19) Pirhashemi, M.; Habibi-Yangjeh, A.; Rahim Pouran, S. Review on the Criteria Anticipated for the Fabrication of Highly Efficient ZnO-Based Visible-Light-Driven Photocatalysts. *J. Ind. Eng. Chem.* **2018**, *62*, 1−25.
(20) Ullah, H.; Mushtaq, L.; Ullah, Z.; Fazal, A.; Khan, A. M. Effect of Vegetable Waste Extract on Microstructure, Morphology, and Photocatalytic Efficiency of ZnO−CuO Nanocomposites. *Inorg. Nano-Metal Chem.* **2021**, *51*, 963−975.
(21) Yendrapati Taraka, T. P.; Gautam, A.; Jain, S. L.; Bojja, S.; Pal, U. Controlled Addition of Cu/Zn in Hierarchical CuO/ZnO p-n Heterojunction Photocatalyst for High Photoreduction of CO_2 to MeOH. *J. CO2 Util.* **2019**, *31*, 207−214.
(22) Sahu, K.; Bisht, A.; Kuriakose, S.; Mohapatra, S. Two-Dimensional CuO-ZnO Nanohybrids with Enhanced Photocatalytic Performance for Removal of Pollutants. *J. Phys. Chem. Solids* **2020**, *137*, No. 109223.
(23) Liu, C.; Meng, F.; Zhang, L.; Zhang, D.; Wei, S.; Qi, K.; Fan, J.; Zhang, H.; Cui, X. CuO/ZnO Heterojunction Nanoarrays for Enhanced Photoelectrochemical Water Oxidation. *Appl. Surf. Sci.* **2019**, *469*, 276−282.
(24) Sandhya, J.; Kalaiselvam, S. UV Responsive Quercetin Derived and Functionalized CuO/ZnO Nanocomposite in Ameliorating Photocatalytic Degradation of Rhodamine B Dye and Enhanced Biocidal Activity against Selected Pathogenic Strains. *J. Environ. Sci. Health, Part A* **2021**, *56*, 835−848.
(25) Velayi, E.; Norouzbeigi, R. Single-Step Prepared Hybrid ZnO/CuO Nanopowders for Water Repellent and Corrosion Resistant Coatings. *Ceram. Int.* **2019**, *45*, 16864−16872.
(26) Vo, N. L. U.; Van Nguyen, T. T.; Nguyen, T.; Nguyen, P. A.; Nguyen, V. M.; Nguyen, N. H.; Tran, V. L.; Phan, N. A.; Huynh, K. P. H. Antibacterial Shoe Insole-Coated CuO-ZnO Nanocomposite Synthesized by the Sol-Gel Technique. *J. Nanomater.* **2020**, *2020*, 1−13.
(27) Podrojková, N.; Patera, J.; Popescu, R.; Škoviera, J.; Oriňaková, R.; Oriňak, A. Pyrolysis Degradation of Cellulose over Highly Effective ZnO and ZnO−CuO Nanocatalysts. *ChemistrySelect* **2021**, *6*, 4256−4264.
(28) Fan, C.; Sun, F.; Wang, X.; Majidi, M.; Huang, Z.; Kumar, P.; Liu, B. Enhanced H_2S Gas Sensing Properties by the Optimization of P-CuO/n-ZnO Composite Nanofibers. *J. Mater. Sci.* **2020**, *55*, 7702−7714.
(29) Zhang, J.; Gao, S.; Wang, G.; Ma, X.; Jiao, S.; Sang, D.; Liu, S.; Mao, M.; Fang, H.; Wang, J. Tunable Fabrication of CuO Nanoplates on ZnO Nanorods: Heterostructure Formation by Photodeposition for Enhanced Photocatalytic Activity. *Eur. J. Inorg. Chem.* **2019**, *2019*, 2654−2660.
(30) Pardakhty, A.; Ranjbar, M.; Moshafi, M. H.; Abbasloo, S. A Systematic Study of ZnO/CuO Core/Shell Nanostructures Pegylated by Microwave Assistant Reverse Micelles (RM) Method. *J. Clust. Sci.* **2018**, *29*, 1061−1068.
(31) Nur, A.; Rofi'uddien, J.; Basir, M. A.; Nazriati, N.; Fajaroh, F. Synthesis of ZnO/CuO Composite by The Electrochemical Method

in The Acetat Acid Solution. Equilibrium. *J. Chem. Eng.* **2018**, *2*, 59−63.
(32) Saravanan, R.; Karthikeyan, S.; Gupta, V. K.; Sekaran, G.; Narayanan, V.; Stephen, A. Enhanced Photocatalytic Activity of ZnO/CuO Nanocomposite for the Degradation of Textile Dye on Visible Light Illumination. *Mater. Sci. Eng. C* **2013**, *33*, 91−98.
(33) Saravanakkumar, D.; Sivaranjani, S.; Kaviyarasu, K.; Ayeshamariam, A.; Ravikumar, B.; Pandiarajan, S.; Veeralakshmi, C.; Jayachandran, M.; Maaza, M. Synthesis and Characterization of ZnO-CuO Nanocomposites Powder by Modified Perfume Spray Pyrolysis Method and Its Antimicrobial Investigation. *J. Semicond.* **2018**, *39*, No. 033001.
(34) Sharifi, M.; Pothu, R.; Boddula, R. Microwave-Assisted Reduction Reactions. In *Green Sustainable Process for Chemical and Environmental Engineering and Science*; Elsevier, 2021; pp 315−330.
(35) Paristiowati, M.; Zulmanelis, Z.; Nurhadi, M. F. Green Chemistry-Based Experiments As the Implementation of Sustainable Development Values. *JTK (J. Tadris Kim.* **2019**, *4*, 11−20.
(36) Ali, S. G.; Ansari, M. A.; Jamal, Q. M. S.; Almatroudi, A.; Alzohairy, M. A.; Alomary, M. N.; Rehman, S.; Mahadevamurthy, M.; Jalal, M.; Khan, H. M.; Adil, S. F.; Khan, M.; Al-Warthan, A. Butea Monosperma Seed Extract Mediated Biosynthesis of ZnO NPs and Their Antibacterial, Antibiofilm and Anti-Quorum Sensing Potentialities. *Arabian J. Chem.* **2021**, *14*, No. 103044.
(37) Adil, S. F.; Assal, M. E.; Khan, M.; Al-Warthan, A.; Siddiqui, M. R. H.; Liz-Marzán, L. M. Biogenic Synthesis of Metallic Nanoparticles and Prospects toward Green Chemistry. *Dalton Trans.* **2015**, *44*, 9709−9717.
(38) Nasrollahzadeh, M.; Sajjadi, M.; Sajadi, S. M.; Issaabadi, Z. Green Nanotechnology. In *Interface Science and Technology*; Elsevier Ltd., 2019; Vol. *28*, pp 145−198.
(39) Marslin, G.; Siram, K.; Maqbool, Q.; Selvakesavan, R. K.; Kruszka, D.; Kachlicki, P.; Franklin, G. Secondary Metabolites in the Green Synthesis of Metallic Nanoparticles. *Materials* **2018**, *11*, No. 940.
(40) Khan, M.; Shaik, M. R.; Adil, S. F.; Khan, S. T.; Al-Warthan, A.; Siddiqui, M. R. H.; Tahir, M. N.; Tremel, W. Plant Extracts as Green Reductants for the Synthesis of Silver Nanoparticles: Lessons from Chemical Synthesis. *Dalton Trans.* **2018**, *47*, 11988−12010.
(41) Ahmed, S.; Annu; Chaudhry, S. A.; Ikram, S. A Review on Biogenic Synthesis of ZnO Nanoparticles Using Plant Extracts and Microbes: A Prospect towards Green Chemistry. *J. Photochem. Photobiol., B* **2017**, *166*, 272−284.
(42) Azizi, S.; Mohamad, R.; Bahadoran, A.; Bayat, S.; Rahim, R. A.; Ariff, A.; Saad, W. Z. Effect of Annealing Temperature on Antimicrobial and Structural Properties of Bio-Synthesized Zinc Oxide Nanoparticles Using Flower Extract of Anchusa Italica. *J. Photochem. Photobiol., B* **2016**, *161*, 441−449.
(43) Bayrami, A.; Parvinroo, S.; Habibi-Yangjeh, A.; Rahim Pouran, S. Bio-Extract-Mediated ZnO Nanoparticles: Microwave-Assisted Synthesis, Characterization and Antidiabetic Activity Evaluation. *Artif. Cells, Nanomed. Biotechnol.* **2018**, *46*, 730−739.
(44) Khan, S. A.; Noreen, F.; Kanwal, S.; Iqbal, A.; Hussain, G. Green Synthesis of ZnO and Cu-Doped ZnO Nanoparticles from Leaf Extracts of Abutilon Indicum, *Clerodendrum Infortunatum*, *Clerodendrum Inerme* and Investigation of Their Biological and Photocatalytic Activities. *Mater. Sci. Eng. C* **2018**, *82*, 46−59.
(45) Bordbar, M.; Negahdar, N.; Nasrollahzadeh, M. *Melissa officinalis* L. Leaf Extract Assisted Green Synthesis of CuO/ZnO Nanocomposite for the Reduction of 4-Nitrophenol and Rhodamine B. *Sep. Purif. Technol.* **2018**, *191*, 295−300.
(46) Mohammadi-Aloucheh, R.; Habibi-Yangjeh, A.; Bayrami, A.; Latifi-Navid, S.; Asadi, A. Enhanced Anti-Bacterial Activities of ZnO Nanoparticles and ZnO/CuO Nanocomposites Synthesized Using *Vaccinium arctostaphylos* L. Fruit Extract. *Artif. Cells, Nanomed. Biotechnol.* **2018**, *46*, 1200−1209.
(47) Thatikayala, D.; Min, B. Ginkgo Leaves Extract-Assisted Synthesis of ZnO/CuO Nanocrystals for Efficient UV-Induced Photodegradation of Organic Dyes and Antibacterial Activity. *J. Mater. Sci. Mater. Electron.* **2021**, *32*, 17154−17169.
(48) Geyid, A.; Abebe, D.; Debella, A.; Makonnen, Z.; Aberra, F.; Teka, F.; Kebede, T.; Urga, K.; Yersaw, K.; Biza, T.; Mariam, B. H.; Guta, M. Screening of Some Medicinal Plants of Ethiopia for Their Anti-Microbial Properties and Chemical Profiles. *J. Ethnopharmacol.* **2005**, *97*, 421−427.
(49) Mergia, E.; Shibeshi, W.; Terefe, G.; Teklehaymanot, T. Antitrypanosomal Activity of *Verbascum sinaiticum* Benth. (*Scrophulariaceae*) against *Trypanosoma congolense* Isolates. *BMC Complementary Altern. Med.* **2016**, *16*, No. 362.
(50) Liu, F.; Che, Y.; Chai, Q.; Zhao, M.; Lv, Y.; Sun, H.; Wang, Y.; Sun, J.; Zhao, C. Construction of RGO Wrapping Cu_2O/ZnO Heterostructure Photocatalyst for PNP and PAM Degradation. *Environ. Sci. Pollut. Res.* **2019**, *26*, 25286−25300.
(51) Zelekew, O. A.; Kuo, D. H. Facile Synthesis of SiO_2@Cu_xO@TiO_2 Heterostructures for Catalytic Reductions of 4-Nitrophenol and 2-Nitroaniline Organic Pollutants. *Appl. Surf. Sci.* **2017**, *393*, 110−118.
(52) Taufique, M. F. N.; Haque, A.; Karnati, P.; Ghosh, K. ZnO−CuO Nanocomposites with Improved Photocatalytic Activity for Environmental and Energy Applications. *J. Electron. Mater.* **2018**, *47*, 6731−6745.
(53) Li, J.; Zhang, Y.; Li, L.; Wang, Y.; Zhang, L.; Zhang, B.; Wang, F. Formation of Dumbbell and Sphere-like CuO as High-Performance Anode Materials for Lithium Ion Batteries. *Mater. Lett.* **2020**, *261*, No. 127058.
(54) Witoon, T.; Permsirivanich, T.; Chareonpanich, M. Chitosan-Assisted Combustion Synthesis of CuO-ZnO Nanocomposites: Effect of PH and Chitosan Concentration. *Ceram. Int.* **2013**, *39*, 3371−3375.
(55) Kirankumar, V. S.; Sumathi, S. A Review on Photodegradation of Organic Pollutants Using Spinel Oxide. *Mater. Today Chem.* **2020**, *18*, No. 100355.
(56) Islam, M. T.; Dominguez, A.; Alvarado-Tenorio, B.; Bernal, R. A.; Montes, M. O.; Noveron, J. C. Sucrose-Mediated Fast Synthesis of Zinc Oxide Nanoparticles for the Photocatalytic Degradation of Organic Pollutants in Water. *ACS Omega* **2019**, *4*, 6560−6572.
(57) Zhu, L.; Li, H.; Liu, Z.; Xia, P.; Xie, Y.; Xiong, D. Synthesis of the 0D/3D CuO/ZnO Heterojunction with Enhanced Photocatalytic Activity. *J. Phys. Chem. C* **2018**, *122*, 9531−9539.
(58) Sathishkumar, P.; Sweena, R.; Wu, J. J.; Anandan, S. Synthesis of CuO-ZnO Nanophotocatalyst for Visible Light Assisted Degradation of a Textile Dye in Aqueous Solution. *Chem. Eng. J.* **2011**, *171*, 136−140.
(59) Yu, J.; Zhuang, S.; Xu, X.; Zhu, W.; Feng, B.; Hu, J. Photogenerated Electron Reservoir in Hetero-p-n CuO-ZnO Nanocomposite Device for Visible-Light-Driven Photocatalytic Reduction of Aqueous Cr(Vi). *J. Mater. Chem. A* **2015**, *3*, 1199−1207.
(60) Xu, L.; Zhou, Y.; Wu, Z.; Zheng, G.; He, J.; Zhou, Y. Improved Photocatalytic Activity of Nanocrystalline ZnO by Coupling with CuO. *J. Phys. Chem. Solids* **2017**, *106*, 29−36.
(61) Lavín, A.; Sivasamy, R.; Mosquera, E.; Morel, M. J. High Proportion ZnO/CuO Nanocomposites: Synthesis, Structural and Optical Properties, and Their Photocatalytic Behavior. *Surf., Interfaces* **2019**, *17*, No. 100367.
(62) Chen, C.; Liu, X.; Fang, Q.; Chen, X.; Liu, T.; Zhang, M. Self-Assembly Synthesis of CuO/ZnO Hollow Microspheres and Their Photocatalytic Performance under Natural Sunlight. *Vacuum* **2020**, *174*, No. 109198.
(63) Lei, X.; Cao, Y.; Chen, Q.; Ao, X.; Fang, Y.; Liu, B. ZIF-8 Derived Hollow CuO/ZnO Material for Study of Enhanced Photocatalytic Performance. *Colloids Surf., A* **2019**, *568*, 1−10.
(64) Zhang, X.; He, X.; Kang, Z.; Cui, M.; Yang, D. P.; Luque, R. Waste Eggshell-Derived Dual-Functional CuO/ZnO/Eggshell Nanocomposites: (Photo)Catalytic Reduction and Bacterial Inactivation. *ACS Sustainable Chem. Eng.* **2019**, *7*, 15762−15771.
(65) Zhang, Z.; Wang, P. Highly Stable Copper Oxide Composite as an Effective Photocathode for Water Splitting via a Facile Electrochemical Synthesis Strategy. *J. Mater. Chem.* **2012**, *22*, 2456−2464.

https://doi.org/10.1021/acsomega.2c02687
ACS Omega 2022, 7, 30908−30919

(66) Zhang, Z.; Sun, L.; Wu, Z.; Liu, Y.; Li, S. Facile Hydrothermal Synthesis of CuO-Cu_2O/GO Nanocomposites for the Photocatalytic Degradation of Organic Dye and Tetracycline Pollutants. *New J. Chem.* **2020**, *44*, 6420−6427.
(67) Taufik, A.; Saleh, R. Synthesis of Iron(II,III) Oxide/Zinc Oxide/Copper(II) Oxide (Fe_3O_4/ZnO/CuO) Nanocomposites and Their Photosonocatalytic Property for Organic Dye Removal. *J. Colloid Interface Sci.* **2017**, *491*, 27−36.
(68) Huang, J.; Yu, K.; Gu, C.; Zhai, M.; Wu, Y.; Yang, M.; Liu, J. Preparation of Porous Flower-Shaped SnO2 Nanostructures and Their Gas-Sensing Property. *Sens. Actuators, B* **2010**, *147*, 467−474.
(69) Bharathi, P.; Harish, S.; Archana, J.; Navaneethan, M.; Ponnusamy, S.; Muthamizhchelvan, C.; Shimomura, M.; Hayakawa, Y. Enhanced Charge Transfer and Separation of Hierarchical CuO/ZnO Composites: The Synergistic Effect of Photocatalysis for the Mineralization of Organic Pollutant in Water. *Appl. Surf. Sci.* **2019**, *484*, 884−891.
(70) Babu, S. G.; Karthik, P.; John, M. C.; Lakhera, S. K.; Ashokkumar, M.; Khim, J.; Neppolian, B. Synergistic Effect of Sono-Photocatalytic Process for the Degradation of Organic Pollutants Using CuO-TiO_2/RGO. *Ultrason. Sonochem.* **2019**, *50*, 218−223.
(71) Huang, F.; Chen, L.; Wang, H.; Yan, Z. Analysis of the Degradation Mechanism of Methylene Blue by Atmospheric Pressure Dielectric Barrier Discharge Plasma. *Chem. Eng. J.* **2010**, *162*, 250−256.
(72) Zelekew, O. A.; Fufa, P. A.; Sabir, F. K.; Duma, A. D. Water Hyacinth Plant Extract Mediated Green Synthesis of Cr_2O_3/ZnO Composite Photocatalyst for the Degradation of Organic Dye. *Heliyon* **2021**, *7*, No. e07652.
(73) Renuka, L.; Anantharaju, K. S.; Vidya, Y. S.; Nagaswarupa, H. P.; Prashantha, S. C.; Nagabhushana, H. Synthesis of Sunlight Driven ZnO/CuO Nanocomposite: Characterization, Optical, Electrochemical and Photocatalytic Studies. *Mater. Today Proc.* **2017**, *4*, 11782−11790.
(74) Mageshwari, K.; Nataraj, D.; Pal, T.; Sathyamoorthy, R.; Park, J. Improved Photocatalytic Activity of ZnO Coupled CuO Nanocomposites Synthesized by Reflux Condensation Method. *J. Alloys Compd.* **2015**, *625*, 362−370.
(75) Kandula, S.; Jeevanandam, P. Synthesis of Cu_2O@Ag Polyhedral Core-Shell Nanoparticles by a Thermal Decomposition Approach for Catalytic Applications. *Eur. J. Inorg. Chem.* **2016**, *2016*, 1548−1557.
(76) Zhao, Y.; Li, R.; Jiang, P.; Zhang, K.; Dong, Y.; Xie, W. Mechanistic Study of Catalytic Hydride Reduction of -NO_2 to -NH_2 Using Isotopic Solvent and Reducer: The Real Hydrogen Source. *J. Phys. Chem. C* **2019**, *123*, 15582−15588.

https://doi.org/10.1021/acsomega.2c02687
ACS Omega 2022, 7, 30908−30919